Chemical imaging of alligatoring oil paintings

Raquel Marques, Caroline Bouvier, Marine Cotte, Alain Brunelle, Emeline Pouyet, Isabel Pombo Cardoso, Leslie Carlyle, Laurence de Viguerie

Chemical imaging of alligatoring oil paintings

Raquel Marques[1,2**], Caroline Bouvier[3**], Marine Cotte[3,4], Alain Brunelle[3], Emeline Pouyet[3], Isabel Pombo Cardoso[1,2], Leslie Carlyle[1,2], Laurence De Viguerie[3*]

[1] Department of Conservation and Restoration, Faculdade de Ciências e Tecnologia, Universidade Nova de Lisboa, Campus da Caparica, 2829-516 Caparica, Portugal

[2] LAQV-REQUIMTE, Faculdade Ciências e Tecnologia, Universidade Nova de Lisboa, Campus da Caparica, 2829-516 Caparica, Portugal

[3] Sorbonne Université, CNRS, Laboratoire d'Archéologie Moléculaire et Structurale, LAMS, 4 place Jussieu,75005 Paris, France

[4] European Synchrotron Radiation Facility (ESRF), 71 avenue des martyrs, 38000 Grenoble, France

**Both authors contributed equally.

Keywords
Alligatoring, lead azelate, ATR-FTIR Microscopy, TOF-SIMS, molecular mapping, painting

Abstract

The so-called "Alligatoring" paint deterioration phenomenon was investigated through the study of four samples from *O Cardeal D. Henrique recebendo a notícia da morte de D. Sebastião*, painted in 1861 by the Portuguese painter Marciano Henriques da Silva. Attenuated Total internal Reflection Fourier Transform Infrared (ATR-FTIR) microscopy and Time-Of-Flight Secondary Ion Mass Spectrometry (TOF-SIMS) imaging, complementary to Scanning Electron Microscopy Energy-dispersive X-Ray spectroscopy (SEM-EDX), were used to tackle the complexity of such paint systems and locate the distribution of organic/inorganic/hybrid components in the paint layers stratigraphy. While the use of asphalt/bitumen commonly associated with this peculiar paint deterioration, was hypothetised, its presence could not be confirmed nor denied with the methodological approach proposed. However, specific chemical compounds and paint layer structures were identified, both related to strong drying issues of the paint system. Most specifically, the evidence of a stable lead azelate layer together with lead and aluminium carboxylates present in all paint layers, combined with a paint technique with numerous paint layer superimposed and an excess of oil in the paint system can be pointed out as clues in the understanding of the degradation mechanisms.

1 Introduction

It is not uncommon to see oil paintings produced during the mid-18th and 19th centuries in Europe exhibiting paint failure in the form of severely disfiguring drying cracks and surface distortions often referred to as "alligatoring" or "bitumen cracking". Considering its negative visual impact, a thorough review of the literature reveals a surprising lack of sustained investigation into this phenomenon. Reported to develop some years after completion of the painting, the degradation has commonly been associated with the use of asphalt/bitumen paint [1,2,3,4] however to date there has been very limited analytical evidence of the use of asphalt/bitumen in affected paintings. The focus on anecdotal evidence of asphalt/bitumen being the cause of "Bitumen cracking" has resulted in a confirmation bias [5] such that the possibility that other materials may be acting in combination or be more predominant in the deterioration mechanism has been largely overlooked. Whether or not asphalt/bitumen is responsible for alligatoring, the failure of efforts to identify it through chemical analyses of paint passages exhibiting this distinctive deterioration can be explained in at least some cases by the finding

that chemical markers for the presence of asphalt/bitumen were lost during heat processing of reconstructions of Bitumen Brown oil paint based on a 19th century commercial production method [6]. A further consideration regarding negative analytical results for this material is that asphalt/bitumen substitutions or new oil processing methods introduced in the mid to late 18th and the 19th centuries may have independently led to the characteristic alligator-skin effect in the paint. Coal-tar derivatives were reported as substitutes for traditional sources of asphalt/bitumen, and drying oil processing using sulphuric acid, and adulterated oils were also reported [7, 8]. While painting techniques such as layering sequence and paint thickness, and choice of materials have been implicated in historical documents both individually or in combination (eg. asphalt/bitumen and gelled Mediums based on mastic varnish), reports on the scientific analyses of these materials and their role in the context of drying problems are scarce.

This article focusses on paint samples taken from an oil painting executed in Rome in 1861 (*O Cardeal D. Henrique recebendo a notícia da morte de D. Sebastião*), by the Portuguese artist Marciano Henriques da Silva (1831-1873). The alligatoring of the paint is so severe that the original image is unintelligible (Figure 1). The paint samples exhibit highly disrupted paint layer stratigraphy (Figure 2), and their composition appeared to be a complex combination of organic and inorganic materials, making chemical analyses challenging. Therefore several imaging techniques were combined: Scanning Electron Microscopy- and Energy-dispersive x-ray spectroscopy (SEM-EDX), Attenuated total internal reflection Fourier transform infrared (ATR-FTIR) microscopy, and time-of-flight secondary ion mass spectrometry (TOF-SIMS). Those techniques have already proven to be particularly relevant to decipher complex paint mixtures, degradation products or alteration mechanisms [9, 10, 11, 12, 13, 14]. However with the exception of work by Keune (e.g. [15]) and Mazel (e.g. [16)] their use in combination has not been widely adopted in the cultural heritage field.

2 Materials and Methods

2.1 Historical painting and samples

The painting *O Cardeal D. Henrique recebendo a notícia da morte de D. Sebastião* (by Marciano Henriques da Silva in 1861) (see Figure 1a) was given as a long-term loan to the DCR in FCT/NOVA for research purposes in April 2014. The surface of the painting exhibits a wide range of defects (Figure 1b to e and Figures S1 and S2): severe wrinkling, paint islands (caused by the contraction of paint, resulting in more elevated areas of paint), exudates, and strong differences in optical properties (some areas being matt whereas others are highly glossy). The brown and red colours are most affected with colours containing lead white being least affected.

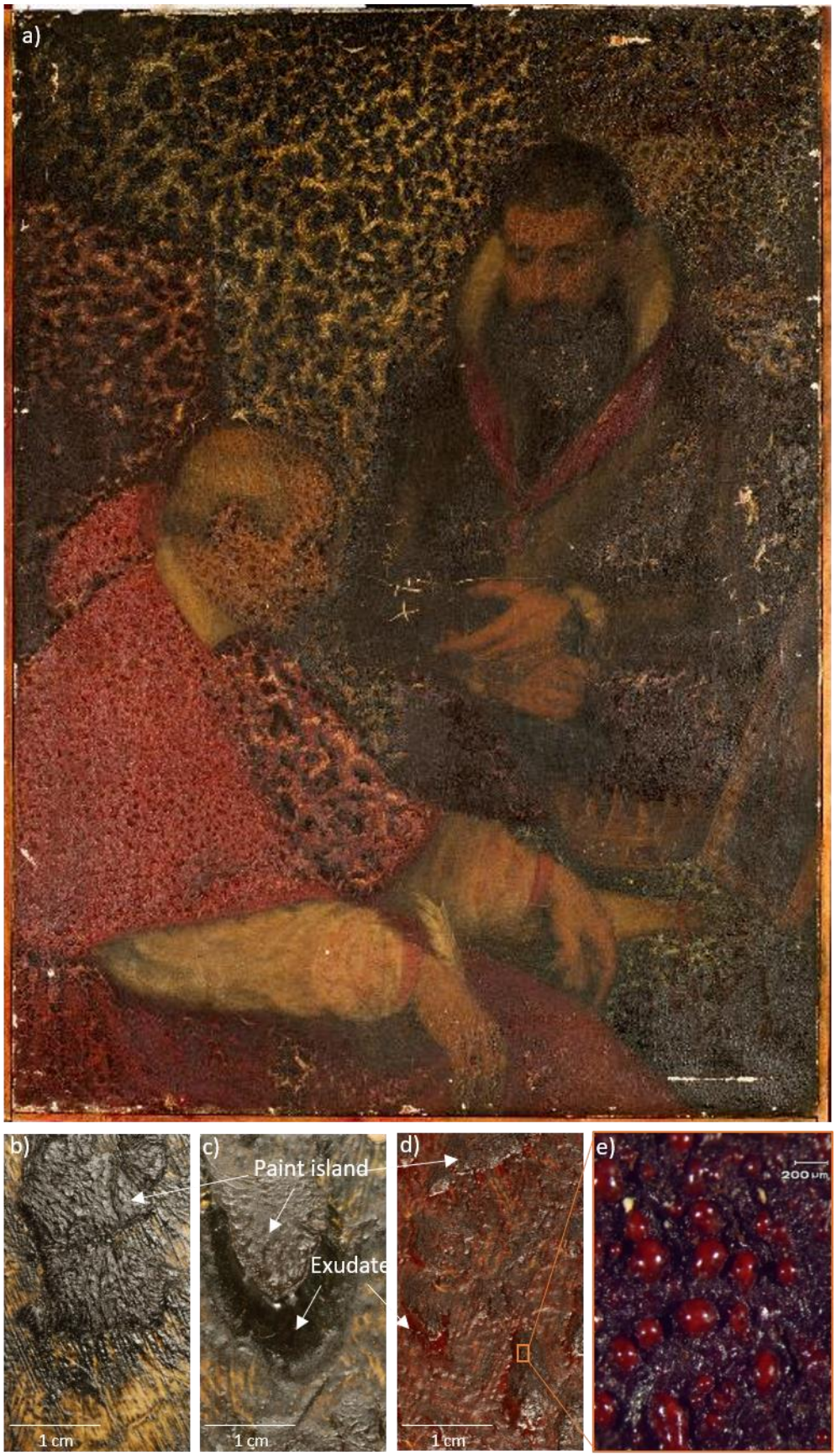

Figure 1: a) Oil painting, *O Cardeal D. Henrique recebendo a notícia da morte de D. Sebastião,* 1861 (137.5 cm x 99.6 cm) by Marciano Henriques da Silva. Overall image showing the severe disfiguration of the image and the uneven gloss/matt paint

surface. Macro-photographs of the paint defects observed: b-d) paint islands, c-d) islands surrounded by exudates, e) small beads protruding from the paint islands.

The samples (S) under consideration in this article were removed from the brown paint (S7 & S19) and from the red paint (S1 & S27), see Figure 2. The sample locations are shown in Figure 2 c). The paint samples were embedded in blocks of polyester resin (MR Dinis Resina Poliester Cristal, from MR Dinis dos Santos). After polishing to expose the sample in cross-section, the resin block and sample were dry polished with a set of Micromesh abrasive sheets. The paint cross-sections were then investigated with an optical microscope in both visible and ultra violet light (UV).

- S7 and S19 from brown paint islands show similar stratigraphy. S19 which has been sampled from the edge of a paint island exhibits two sections: one from flat area (left side, figure 2b) and the other one from the paint island (right side, figure 2b) with an upper moving layer, fluorescent under UV (indicated by an arrow in figure 2b).
- S1 and S27 from red paint islands, S1 exhibits two visible paint layers, while S27 exhibits multiple paint layers which are distorted into a series of wave-like bands of paint (the UV image shows at least 10 paint layers present).

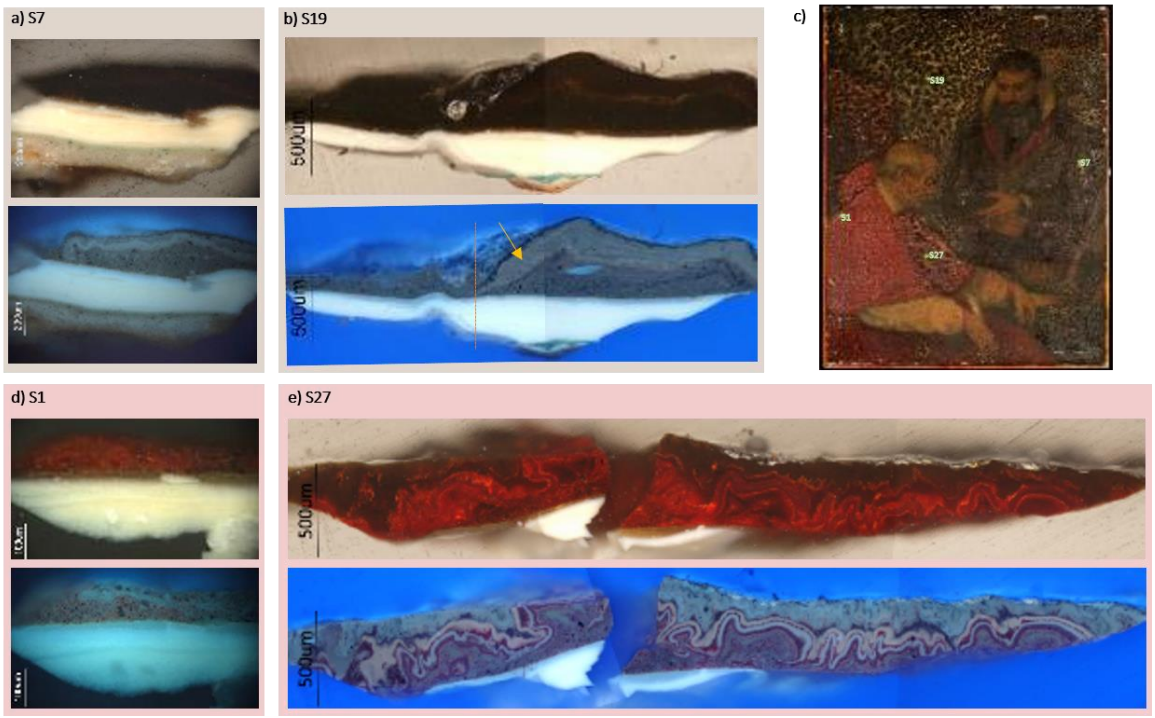

Figure 2: a), b), d) and e): Cross-sections S7 (a), S19 (b), S1 (d) and S27 (e) in cross-polarised light (upper image) and under UV (lower image). c): Painting under study with green marks indicating the sampling locations of each cross-section.

The samples were then all investigated with SEM-EDX. ATR-FTIR microscopy was used to investigate samples S1 and S7; while S19 and S27, of higher structural complexity and containing thinner layers, were investigated by TOF-SIMS imaging to achieve higher lateral resolution. To be able to compare the two sets of samples, complementary specific point µ-FTIR spectroscopy was carried out on samples S19 and S27 and an additional TOF-SIMS imaging analysis was performed on sample S7.

2.2 Imaging techniques

2.2.1 Optical Microscope (all samples)

Analyses were carried out in an Axioplan 2ie Zeiss microscope equipped with a transmitted and incident halogen light illuminator (tungsten light source, HAL 100); incident UV radiation (mercury light source, HBO 100 illuminator); and a digital Nikon camera DXM1200F, with Nikon ACT-1 application program software, for microphotographs. Samples were analysed with 10x ocular lenses and 5x/10x/20x/50x objective Epiplan lenses (giving total optical magnification of 50x, 100x, 200x, and 500x). For the incident and transmitted light (normal light) the samples were analysed under cross polars – polariser and analyser filters; and for UV radiation the Zeiss filter set 2 [BP300-400, FT 395, LP 420] was used. The scales for all lenses were calibrated within the Nikon ACT-1 software.

2.2.2 SEM-EDX (all samples)

Scanning Electron Microscopy/energy-dispersive X-Ray spectroscopy, imaging and microanalysis were performed on a Hitachi SU-70 FEGSEM (Schottky emission gun), fitted out with an X-Max 50mm^2 Oxford EDX spectrometer. The Oxford spectrometer software used was first INCA and later AZTEC after an update. Prior to analyses all samples were carbon coated (estimated thickness 40 nm) to ensure the presence of a conductive layer on top and to consequently enable or improve the imaging of the samples which are otherwise insulating.

2.2.2 FTIR-ATR microscopy (samples S1 and S7)

The FTIR-ATR analyses were performed using a Perkin Elmer Spectrum 100 FTIR spectrometer combined with a Spectrum Spotlight 400 FTIR microscope equipped with a 16x1 pixel linear mercury cadmium telluride (MCT) array detector. A Perkin Elmer ATR imaging accessory consisting of a germanium crystal was used for ATR imaging. The spectral resolution was 8 cm^{-1}. The map size was 200 × 200 µm² and the lateral resolution 1.5 µm/pixel. Maps were analyzed using the PyMCA ROI imaging package [17]. Briefly, chemical maps were obtained by the integration of the FTIR intensity over different regions of interest (ROI) (see below grey rectangles in figure 3a, b, c). Then, FTIR average spectra were calculated from the different locations by selecting pixels (brush tool) in the most intense parts of the ROI maps.

2.2.3 µ-FTIR spectroscopy (S19 and S1)

Infrared spectra were acquired using a Nicolet Nexus spectrophotometer coupled to a Continumm microscope (15x objective) with a MCT-A detector cooled by liquid nitrogen. The spectra were collected in transmission mode, between 4000 and 650 cm^{-1}, in 50-100 µm areas, with a resolution setting 4 cm^{-1} and 128 or 256 scans, using a Thermo diamond anvil compression cell. When necessary, the system was purged with nitrogen prior to the data acquisition.

2.2.4 TOF-SIMS imaging (samples S7, S19 and S27)

The instrument used was a TOF-SIMS IV (IONTOF GmbH, Germany) located in the Laboratory of Molecular and Structural Archaeology (LAMS, CNRS – Sorbonne University, Paris, France). The primary ion source used for analysis is a liquid metal ion gun delivering a pulsed bismuth cluster ion beam (25 keV energy Bi_3^+ ions) hitting the surface with an incidence angle of 45°, with a low energy electron flood gun neutralizing the surface between each scan. The time-of-flight analyzer is equipped with delayed extraction of secondary ions, which permits the combination of a high lateral resolution with a mass resolution of a few thousand, thanks to the so-called “burst alignment with delayed extraction” (BA+DE) focusing mode in which the beam diameter is reduced down to 400 nm. This was described by Vanbellingen *et al*. [18].

The mass spectrometer is also equipped with an argon Gas Cluster Ion Beam (GCIB), which allows a gentle sputtering of the surface without damaging the underlying layers. Before all analyses, a 1000

µm size square surface around the areas of interest was cleaned with a dose of 1.10^{15} ions/cm² using argon clusters of 2000 atoms with a total energy of 10 keV. This way, potential surface contaminants (exogenous lipids or polydimethylsiloxane) were sputtered away. Another interesting use of the GCIB is the possibility to perform a soft sputtering of the surface between each analytical scan, which results in "dual beam" imaging. This yields successive images of the same surface, combining in-depth information and high-lateral resolution surface imaging. Dual beam imaging is adapted for the identification of the chemical nature of sub-micrometric inorganic pigments particles thanks to its high signal intensity. However, the sputtering steps can lead to a selective loss of the organic signals (such as from dyes) in inhomogeneous organic-inorganic surfaces like painting samples. The analysis parameters can be optimized for the detection of organic materials by "locally-tuned imaging" without GCIB sputtering, as described in the literature [19]. Both types of analysis were combined to maximize the chemical information obtained. Dual beam imaging was performed on areas of 400 × 400 µm², separated in 1024 × 1024 pixels, so the pixel size equaled 390 nm. The Bi_3^+ primary dose was 5.10^{12} ions/cm², and the sputtering dose was 1.10^{14} ions/cm². The data obtained were well-contrasted images of inorganic features such as pigments particles, with the thinnest layers precisely located. Complementary data for the organic materials were obtained using locally-tuned imaging on areas of 200 × 200 µm² using a primary ion dose of 5.10^{12} ions/cm². All data were acquired using SurfaceLab 6.7 software (IONTOF GmbH, Germany) and processed with SurfaceLab 7.0.

3 Results

Optical microscope observations of all of the cross sections taken from the painting (in addition to the 4 samples discussed in this article) showed that the stratigraphy is consistent throughout the paint samples. Clearly evident is a prior painting with a distinctive stratigraphy consisting first of a sizing layer of animal glue, a preparation (ground) layer and a series of paint layers (which vary depending on the sampling location). On top of this prior painting is another preparation layer (ground) referred to as the upper ground layer which is followed by a translucent layer which is in turn followed by the paint layers associated with the current painting. Both the brown and red paints consist of multiple layers which could be distinguished with cross-polarised light and under UV radiation (Figure 2).

Regarding the 4 paint samples under discussion, the analytical results are given for the binder identification (common to the whole paint stratigraphy), followed by: 1) the white upper ground layer, 2) a "translucent" layer and 3) the brown and red paint layers respectively.

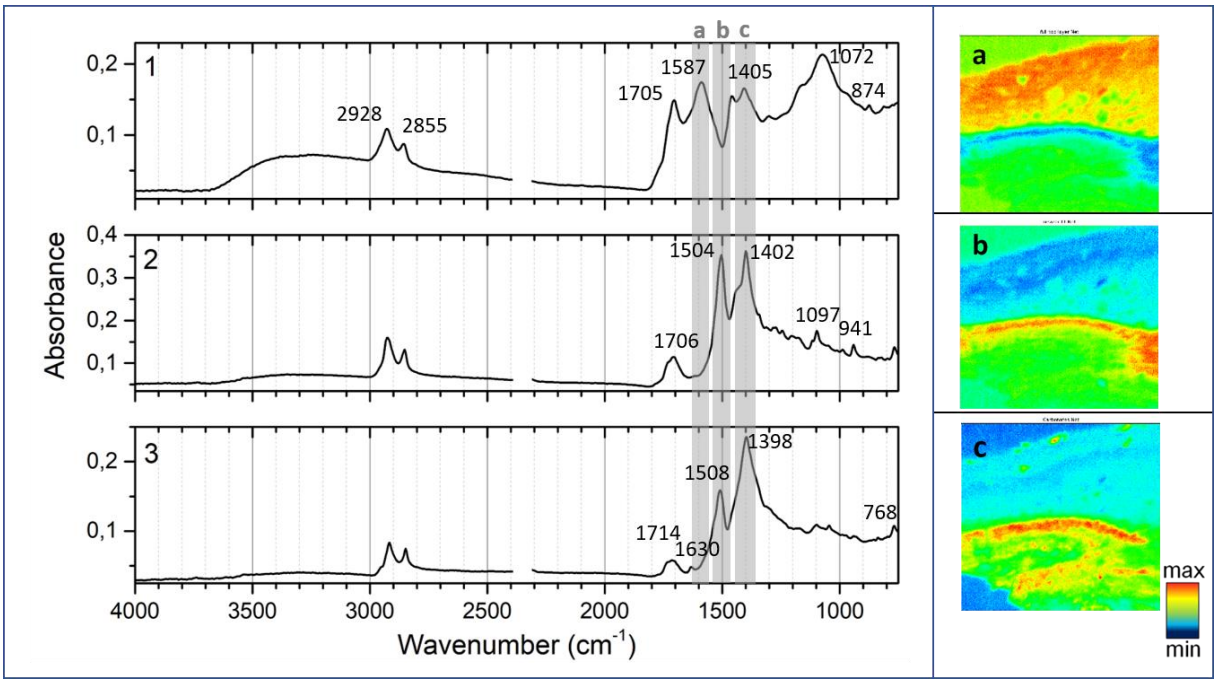

Figure 3: ATR-FTIR microscopy analysis of S7 (brown paint sample). Spectra 1, 2 and 3 were acquired from the maximum values (in red) of the chemical maps a, b and c: a) the top layer (intensity from 1663 to 1501 cm^{-1}), b) the "translucent" layer (intensity from 1557 to 1478 cm^{-1}) and c) the upper ground layer (intensity from 1468 to 1332 cm^{-1}).

3.1 Binder

TOF-SIMS imaging indicated the presence of oil, saponified to some extent, identified through the co-localized detection of fragment ions coming from both oil and lead carboxylates in both polarities. FTIR spectra confirms the presence of oil as a binder with characteristic peaks at 2928 and 2855 cm^{-1} assigned to the C-H stretching vibrations and a carbonyl band that appeared shifted from the expected 1740 cm^{-1} [20, 21, 22] to lower wavelengths with values between 1715 and 1700 cm-1. This shift can be due to the presence of a natural resin (such as mastic or dammar) [23] or to a mixture of oil and resin [24]. As no resin could be detected by TOF-SIMS (or by GC-MS, an on-going study not presented here), it is more likely that this is due to the high degree of hydrolysis of the oil [22]. This result will be checked in future chromatographic investigations since the presence of mastic resin is expected according to the published artists' formulations for bitumen brown oil paint as well as the commercial production records from a leading 19th century colourman [25].

Specific observations from the different paint layers are detailed below. The palmitate (P) over stearate (S) ion ratio (P/S), can be used in the binder characterization using TOF-SIMS [26]. The P/S ratio was estimated for all layers in sample S19 (see Table S1). This ratio was calculated from TOF-SIMS reconstructed spectra extracted from ROIs in each layer. Although not quantitative, this technique is valid as both palmitate and stearate ions behave in the same way under the effect of the primary ion impact (desorption and ionization) and are detected with the same efficiencies, having similar *m/z* values so. The calculated P/S ratio thus retain their initial proportion [27].

3.2 Upper ground layer

In the white upper ground layer, SEM-EDX indicated the overall presence of lead (Figure S3) and ATR-FTIR microscopy indicated a mixture of lead white (hydrocerussite $2PbCO_3.Pb(OH)_2$, cerussite $PbCO_3$) and lead carboxylates (Figure 3c):

- The peaks at 1398 and 1045 cm^{-1} are due to the stretching of the carbonate ion (asymmetric and symmetric bands, respectively), the small band at 3536 cm^{-1} comes from the hydroxyl stretch of lead white – hydrocerussite [28], and the small peak at 838 cm-1 has been assigned to cerussite [22] .
- The sharp peak at 1508 cm^{-1} is characteristic of lead carboxylates.

TOF-SIMS imaging achieved finer details regarding the chemical composition of this white ground layer. The overall layer varies between 150 and 200 µm and characteristic ions for lead carbonate were detected throughout along with the fatty acid ions from oil: lead palmitate and a weaker signal of lead stearate (*m/z* 463.2, $PbC_{16}H_{31}O_2^+$ and *m/z* 491.2, $PbC_{18}H_{35}O_2^+$, respectively). Chloride ions were also detected with different intensities depending on the zone (seen also by SEM-EDX). TOF-SIMS results can be divided into several largely horizontal regions within the white upper ground with variable proportions of carboxylates, lead chlorides and lead carbonate fragments, as shown in Figure 4. A 30 µm thick region in the middle of the ground exhibits a more significant lead carbonate detection whereas others are richer in chlorine content. The presence of chloride, often found associated with lead white pigments [13, 15] is difficult to interpret without further information (either or both production methods or degradation processes may be involved).

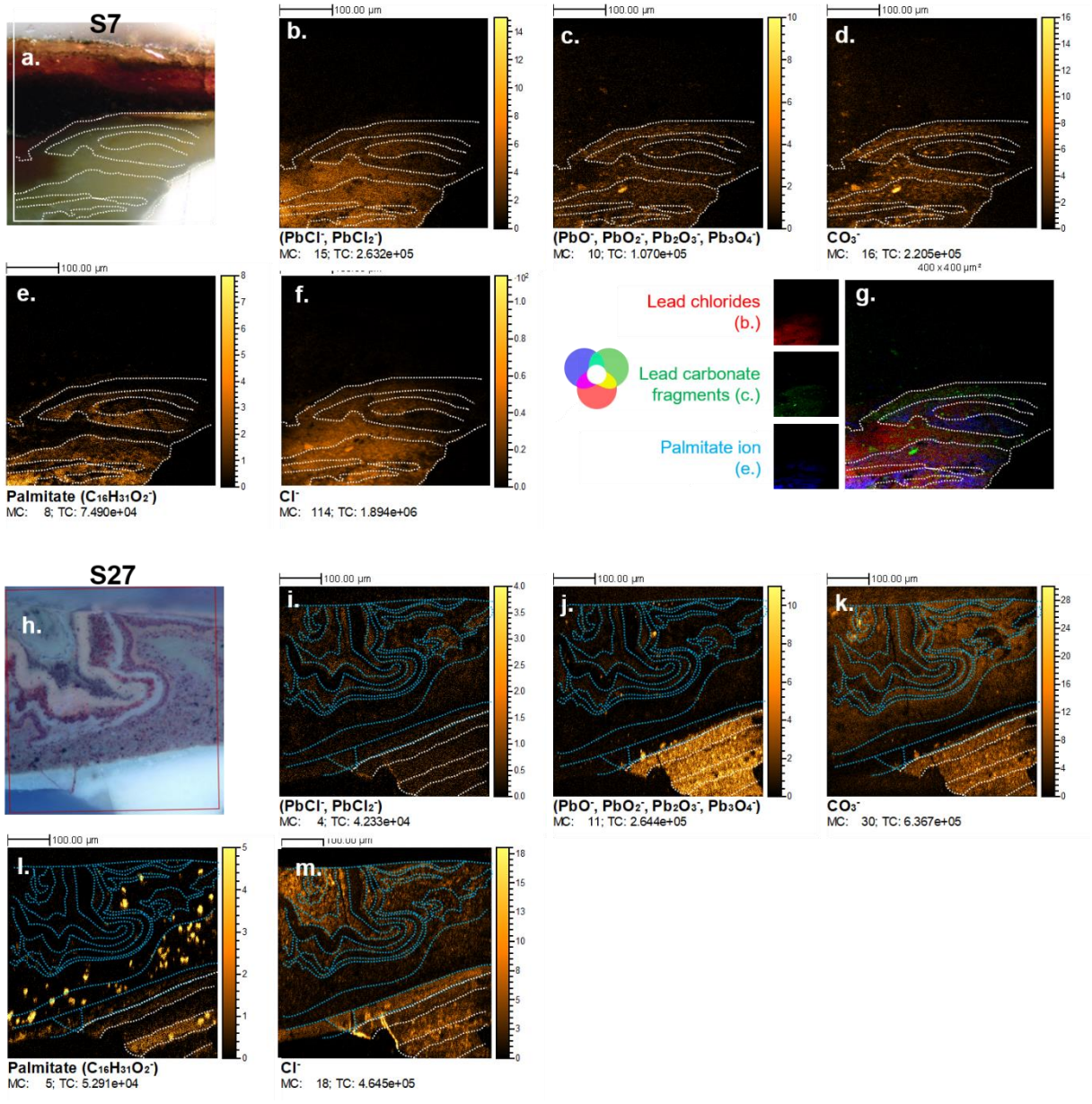

Figure 4: Optical image (a), ground layer regions are delineated between the white dotted lines. TOF-SIMS ion images on sample S7 for (b) lead chlorides ($PbCl^-$ and $PbCl_2^-$), (c) lead white fragments (PbO^- and $Pb_nO_{n+1}^-$), (d) carbonate ion (CO_3^-), (e) palmitate ion ($C_{16}H_{31}O_2^-$) and (f) chloride ion Cl^-, with the overlay of (b. c. and e.) in (g); and UV image (h) and the same TOF-SIMS ion images for sample S27 (i) to (m).

3.3 Translucent layer

A distinctive translucent layer is visible above the upper lead white ground layer in all four samples investigated. Due to its location and limited thickness, this layer was extremely hard to sample. With the imaging techniques used for this research it was possible to decipher the translucent layer's chemical composition without interference from the other layers. ATR-FTIR microscopy provided chemical mapping, integrating the peak at 1504 cm^{-1} (Figure 3b). The average spectrum in the layer shows characteristic peaks for lead azelate (a dicarboxylate saturated C9 fatty chain, $C_9H_{14}O_4Pb$) at 1504, 1444 and 1402 cm^{-1} (Figure 3b and S4) [29]. The presence of lead azelate was confirmed by TOF-SIMS analysis (Figure 5), with the detection of lead azelate ion (PbC9H14O4-, *m/z* 394.07), together with PbOC9H13O4-, *m/z* 409.05 and PbCOC9H13O4-, *m/z* 421.05 ions.
It can also be underlined that the proportion of saturated fatty acids and lead carboxylate ions is higher than in the surrounding layers. Moreover, the local value for the P/S ratio is lower (stearate ion being over-represented compared to palmitate) and the relative proportion of unsaturated (CnH2nO2) versus saturated carboxylate fragments (CnHmO2, with 2n-2 or 2n-4) is higher. To date, the exact significance of these differences has yet to be elucidated, but these results highlight the particularity of this layer in terms of composition, probably linked to specific ageing processes.

The origin of the presence of this layer in the painting is unclear but the assumption of the degradation of an oil layer applied to the ground prior to painting can be made. The application of a layer of oil to the surface of the ground or paint was described routinely in 19th century documentary sources on oil painting materials and techniques either to seal an absorbent ground, or to facilitate paint applications over dried oil grounds or paint [30, p.205-206]. What is particularly puzzling is the predominance of lead azelate in this layer, for which there is to date, no explanation. However its stability has been addressed in the literature: Plater et al. [31] argued that "the higher polarity of azelaic acid and its lead salt, resulting from the shorter hydrocarbon chain and the two carboxylic acid groups, will make these components much less mobile than the monocarboxylic fatty acids". Being less mobile and more stable in a 3D metal coordinated network [35] than monocarboxylates, it is likely that azelaic acid based components would remain as a single layer. The resistance of this layer to the movement and distortion which is seen in the paint layers above is likely explained by its chemistry.

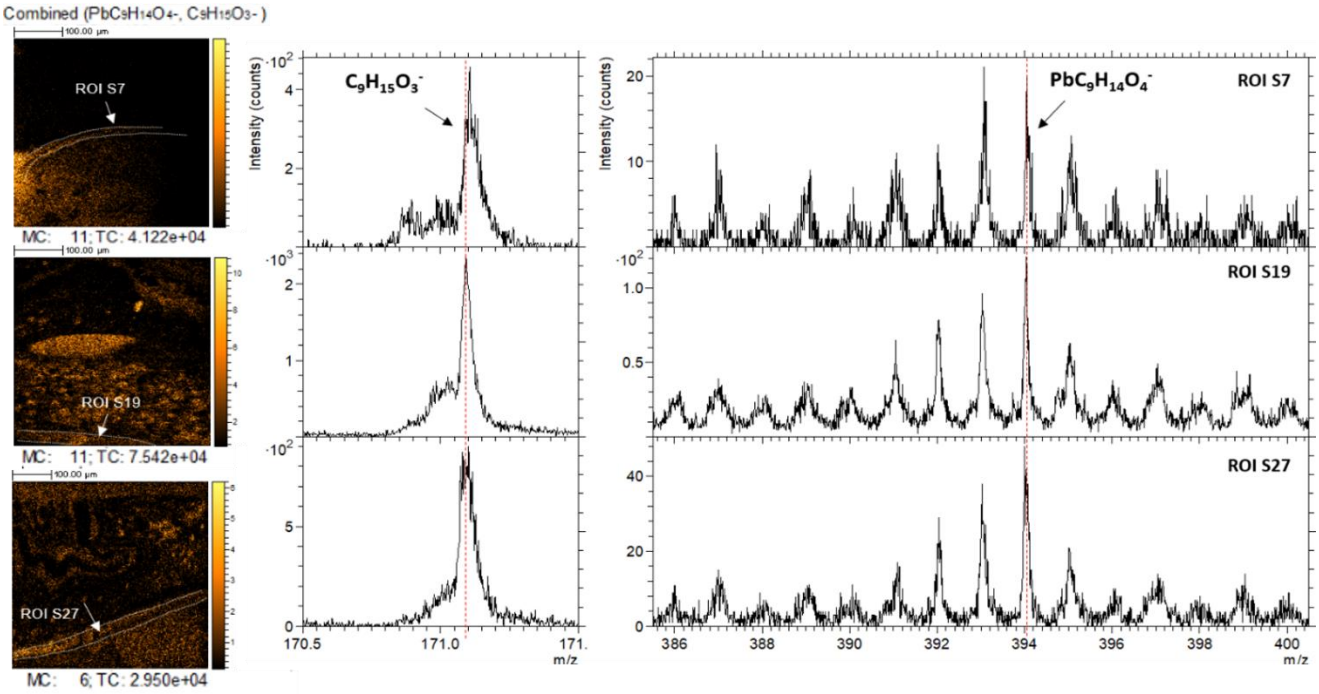

Figure 5: Images of the sums of $PbC_9H_{14}O_4^-$ (lead azelate), *m/z* 394.07, with $C_9H_{15}O_3^-$ *m/z* 171.10 and parts of corresponding mass spectra for three cross-sections.

3.4 Paint layers

3.4.1 Red paint layers: samples S1 and S27

Red paint samples, S27 and S1 were both investigated: although S27 exhibits a much more complex stratigraphy with numerous thin paint layers, their composition appears to be consistent between both samples. The characteristic UV fluorescence of red particles indicates the presence of lake pigments. This was confirmed in SEM-EDX maps (Figure 6) which show aluminium and sulphur associated with the fluorescent particles. Mercury was also detected by SEM-EDX and TOF-SIMS in different layers indicating the use of vermilion (HgS).

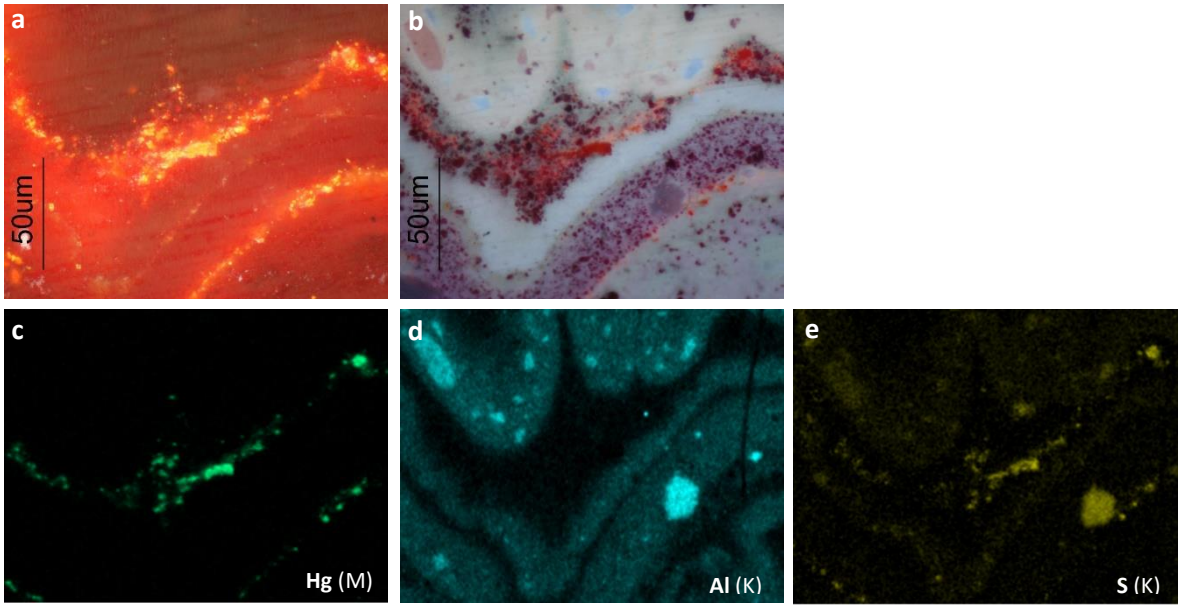

Figure 6: Detail of S27, (a) in cross-polarised light (b) under UV light. EDX elemental mappings of c) mercury (vermilion pigment), d) aluminium, e) and sulphur.

TOF-SIMS imaging provided complementary information. A detailed description of the compounds identified in the different layers of S27 by TOF-SIMS is presented in the supplementary information (Table S2). The ions detected indicated the presence of several aluminium compounds, such as alumina (aluminium oxide) and alum (potassium aluminium sulphate), providing information on the lake manufacture [32]. With the adjusted conditions of locally-tuned imaging, less destructive for organic materials (see Experimental), it was possible to detect characteristic ions from lake chromophores: characteristic ions for madder lake were detected in the mass spectra reconstructed from only a few lake particles. Due to their low secondary ion signal intensity, it was however not possible to obtain a well contrasted image.

No signal in TOF-SIMS related to the oil binder was detected in some of the upper layers in sample S27. However with point measurements using ATR-FTIR microscopy, evidence for oil was detected. This finding provides crucial analytical clues regarding the correct interpretation of TOF-SIMS data in the case of lake rich oil paints. The lack of an oil signal in TOF-SIMS is thought to be related to the presence of aluminium in combination with the absence of lead in these layers. This can be seen in the overlay image of Al and Pb ions (Figure 7). Indeed, the local chemical environment can impact the detection of given ions: lead is known to enhance the fatty acid signal and it may be that aluminium hinders it. Another hypothesis would be that the chemical structure of an oil binder (polymeric/ionomeric network) in the presence of lake pigments results in as yet unidentified unusual secondary ions. Further studies of dried oil paint reconstructions with high aluminium content would be of interest to explore this hypothesis, with analyses performed with a mass range exceeding 800 u.

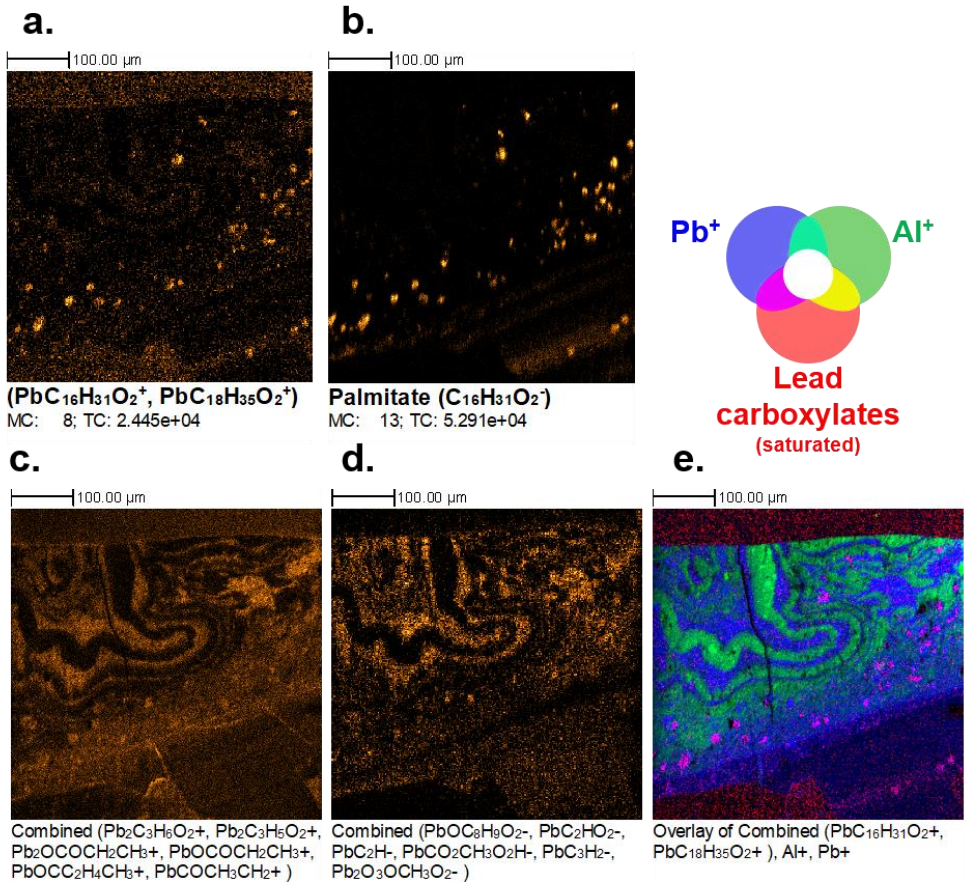

Figure 7: TOF-SIMS ion images for sample S27 of (a) lead carboxylates (stearate $PbC_{18}H_{35}O_2^+$, *m/z* 491.24, and palmitate $PbC_{16}H_{31}O_2^+$, *m/z* 463.21), (b) palmitate ion ($C_{16}H_{31}O_2^-$, *m/z* 255.23), (c) sum of several fragment ions originating from of saponified oil in positive and (d) negative polarities, and (e) three color overlay between lead carboxylates (in red), aluminium ion (in green) and lead ion (in blue).

3.4.2 Brown paint layers

Preliminary analysis of reference paints containing asphalt [6, 33] failed to identify reliable markers for the detection of asphalt/bitumen: bitumen produces fragment ions in TOF-SIMS, which are common to almost all organic matter and lake materials. Consequently, neither FTIR nor TOF-SIMS were able to prove its presence with certainty in these samples. Below we detail the identification of other materials, whose presence and possible importance are often overlooked in the case of paintings suffering from alligatoring.

S7 and S19, samples from brown paint were both investigated by SEM-EDX which revealed the unexpected presence of numerous particles containing aluminium and sulphur, pointing to the presence of yellow/brown lake pigments. The different proportions of Al and S but also K and P appear to indicate a difference in the nature or origin of the lake pigments: Al and S may be associated with the pigment substrate, and K and P with the source of the dyestuff [32]. The description of each layer in S7 is detailed in Table S3.

FTIR data show the presence of metal carboxylates (Figure 8). Further investigation of their distribution in the stratigraphy was made using TOF-SIMS, through the images of lead carboxylates (palmitate and stearate) and carboxylates ions, that would originate from the metal soaps. The combined results of locally-tuned imaging on S7, and dual beam imaging on S7, S19 and S27, demonstrate that for the three samples, lead carboxylates (C_{16} and C_{18}) are concentrated in rounded areas circa 10-20 µm in diameter. These rounded areas are found in the dark layer immediately above the translucent layer. They also appear below the distorted layers in S19 and S27, as shown in Figure 7, Figure 8c, and Figure 9. They are particularly visible using dual beam imaging allowing in-depth profiling, suggesting a lead carboxylate spherical-like distribution. In sample S7 only, aluminum palmitate could also be detected in a single rounded area (Figure S5) which implies that the aluminum complexed with the oil binder forming an aluminum carboxylate.

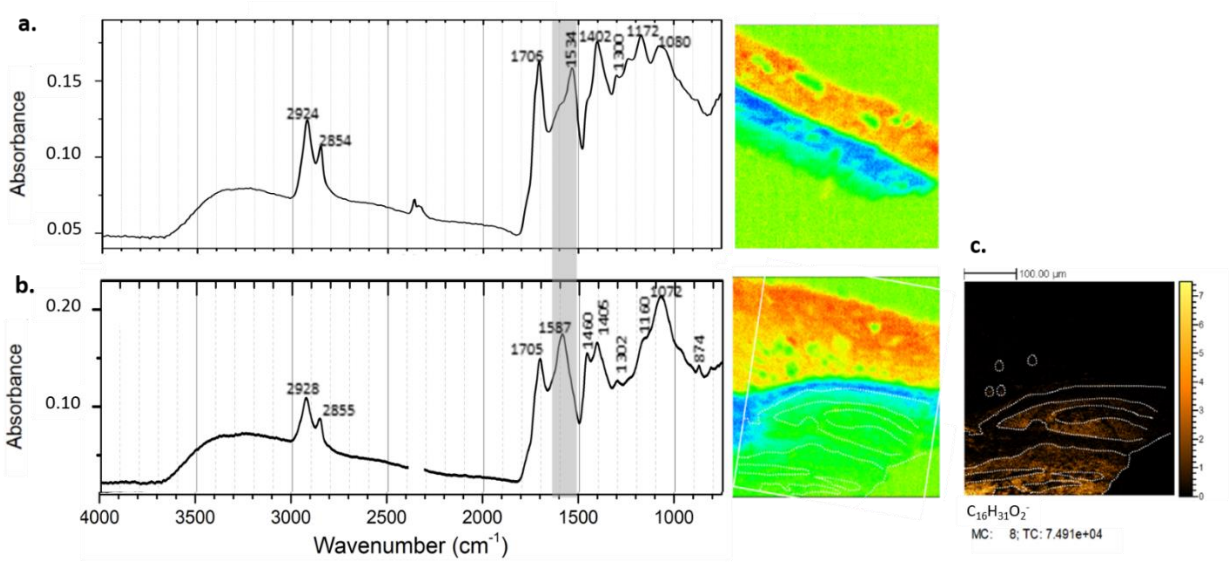

Figure 8: (a) Chemical map **a** of sample S1 (intensity from 1680 to 1498 cm^{-1}), (b) chemical map **a** of sample S7 (intensity from 1663 to 1501 cm^{-1}) and (c) TOF-SIMS ion image for palmitate ion $C_{16}H_{31}O_2^-$, *m/z* 255.23, for sample S7.

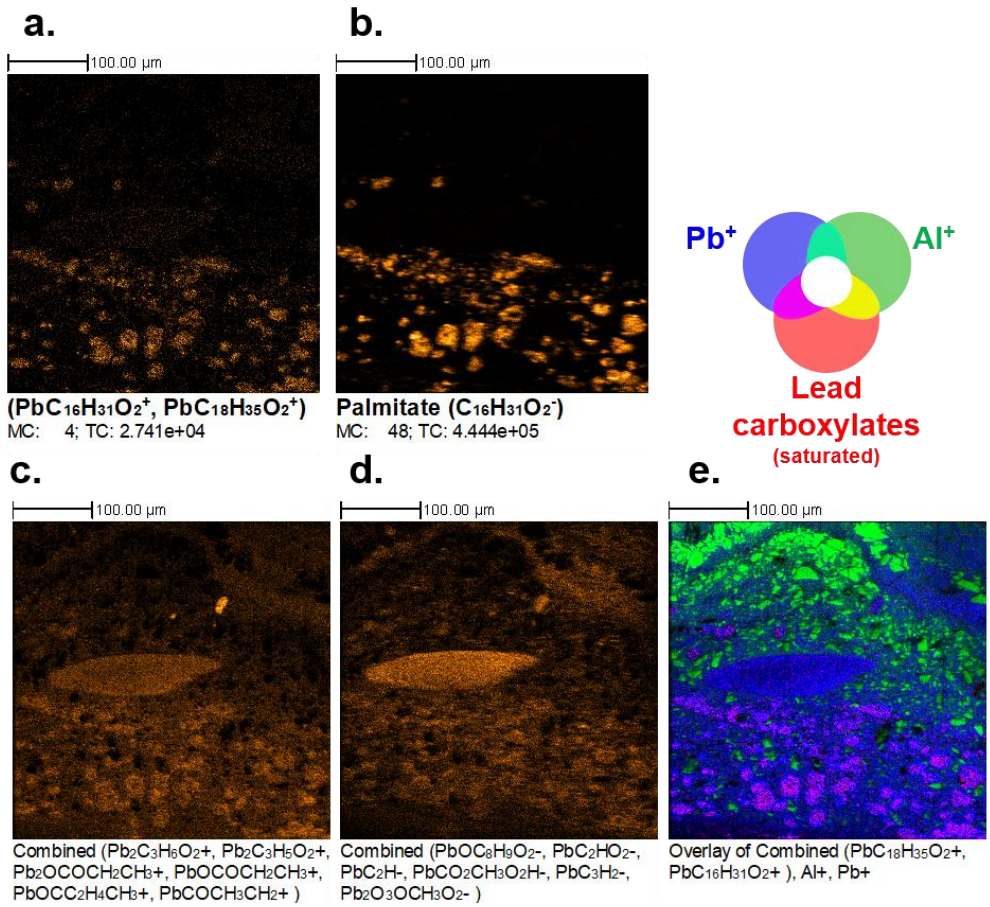

Figure 9: TOF-SIMS images for sample S19: a) lead carboxylates (stearate $PbC_{18}H_{35}O_2^+$, *m/z* 491.24, and palmitate $PbC_{16}H_{31}O_2^+$, *m*/z 463.21), b) palmitate ion ($C_{16}H_{31}O_2^-$, *m/z* 255.23), c) sum of several fragment ions originating from saponified oil in positive polarity and d) in negative polarity, and e) a three color overlay of lead carboxylates (in red), aluminum ion (in green) and lead ion (in blue).

4. Discussion

Advanced imaging techniques were used to provide data from both organic and inorganic materials in the paint samples chosen. By using complementary imaging techniques, interesting and possibly significant results were obtained which points to the highly complex mixture of materials present in the paint and the possible role of lake pigments which may have contributed, in combination or alone, to the severe alligatoring visible in the painting.

Complementary techniques are required to extract meaningful results from the data, particularly when interpreting large datasets comprising ambiguous features as experienced with TOF-SIMS imaging. By combining the two TOF-SIMS imaging approaches, the possibilities of the technique were fully exploited. Locally tuned imaging allowed a more homogeneous detection of organic compounds but negatively impacted the detection of inorganic materials. In addition, all materials were not similarly impacted which can change the detection of markers associated with organic binders or dyes. It is therefore crucial to be aware of the specific limitations of each locally tuned image to meaningfully interpret the data. In particular, identification of hydrocarbon-based compounds yielding no specific markers cannot be unequivocal using TOF-SIMS alone.

This must be emphasised in the case of asphalt/bitumen that could not be detected in these samples, as neither FTIR nor TOF-SIMS can be used to identify it unambiguously. No other material mentioned in the literature in association with alligatoring, like resins, balsams or waxes was found in the painting with FTIR and TOF-SIMS.

If the possible use of asphalt/bitumen could not be confirmed nor denied, we also have to be cautious concerning the presence of mastic resin that could not be detected by TOF-SIMS: we cannot exclude the possibility that the ageing of the paint prevented the resin from being identified in such a complex mixture (it was successfully detected in previously analysed paint reconstructions [25], unpublished results).

However this study revealed several features that may be related to severe alligatoring:

The painting technique involving the superimposition of multiple layers of paint containing lake pigments may in itself have contributed to drying problems since lakes are notoriously slow driers. The presence of a previous painting below the current image may also have contributed to problems since oil binder is normally absorbed into the preparation layers during painting, and multiple dried layers from the first painting may have rendered the paint particularly non-absorbent. This could have left the current painting with a relatively high ratio of oil to pigment, exacerbating drying problems associated with the lakes. Another contribution to the non-absorbent substrate could be the translucent lead azelate layer although its role is far from clear.

Regarding the presence of lake pigments in significant quantities, Shimazu [34] linked a high quantity of lake pigments with a substrate of potassium aluminum sulphate (alum) "to poor drying conditions of oil components" because this material "has a characteristic feature of releasing protons by hydrolysis" [34, p. 169].

Chemical analyses of the binder reported in this paper does appear to confirm a high degree of oil hydrolysis (indicated by the shift in the carbonyl band in ATR-FTIR) supporting the role of lake pigments in relation to oil hydrolysis and leading to the formation of high amounts of carboxylates: lead azelate, forming a stable layer, but also lead monocarboxylates such as lead palmitate or stearate. This overall presence of lead monocarboxylates has been evidenced in all paint layers, dispersed or gathered in some round-shaped regions. Previous research has shown that monocarboxylates are mobile within oil paint systems and contribute to an increase in polarity of the paint, as “monocarboxylic acids can only act as chain terminating units" [35]. This in turn may prevent the formation of a stable 3D network. The combination of these factors may have contributed to the formation of highly polar paint layers. Judging from the layer distortion evident in samples S19 and S27, it is apparent that the paint had been slow to form a solid network.

5. Conclusion

The combination of chemical imaging techniques, SEM-EDX, FTIR Microscopy and TOF-SIMS, has proven extremely useful to investigate the complex stratigraphy of the four cross-sections investigated, not only in the identification of the materials but particularly showing their location within the paint structure.

While the techniques did not lead to a positive identification of markers for asphalt/bitumen in the samples, it would be of interest to continue this work and evaluate whether trace materials or sulfur containing materials from asphalt/bitumen sources could act as markers. Further analyses of the 19th century bitumen brown oil paint reconstructions [6], would be worthwhile in this regard and to

complete the existing extensive TOF-SIMS database of paint material references which made this study possible [14].

The multi-analytical approach identified the presence of significant quantities of lake pigments in the brown and red paint regions most affected by alligatoring, but also lead and aluminium carboxylates. Further work is underway to propose a complete degradation mechanism, but with these findings it can already be assumed that the deterioration of the paint is related to an abundance of polar compounds, and to the oil being heavily hydrolyzed combined with a lack of pigments capable of stabilizing them. Comparison with studies of 20th century dripping oil paints rich in polar fatty acids and diacids [36] will be considered in future chromatographic investigations of the paint samples to evaluate whether the phenomenon of dripping paint has any relationship to the formation of paint islands in alligatoring. Both phenomena have been reported to occur years after the completion of the painting, which may be significant.

Acknowledgements
This work has been funded thanks to the CORES Ph.D. programme PD/00253/2012 and LAQV-Requimte UID/QUI/50006/2019. Special thanks to David Montero for the rewarding SEM sessions for which we thank IMPC FR2482 and Sorbonne Université, CNRS and C'Nano projects. The authors are very grateful to Museu Nacional de Arte Contemporânea – Museu do Chiado, for allowing the painting *O Cardeal…* to be studied in the context of Raquel Marques PhD thesis. ATR-FTIR analyses were carried out at University of Amsterdam, with the support of Joen Hermans and Lambert Baij. We thank Dr. Otero for providing the reference spectrum of lead azelate, and Dr. Jaap Boon for the invaluable help with the data interpretation.

Data availability statement

The datasets generated during and/or analysed during the current study are available from the corresponding author on reasonable request.

References

[1] R. White, National Gallery Technical Bulletin **10**, 58–71 (1986)

[2] L. Carlyle, A. Southall, in *Robert Vernon's Gift, British Art for the Nation 1847* (Tate Gallery Publications, Millbank, 1993), pp. 21–26

[3] G.M. Languri, Molecular Studies of Asphalt, Mummy and Kassel Earth Pigments, Their Characterisation, Identification and Effect on the Drying of Traditional Oil Paint, University of Amsterdam, 2004. https://hdl.handle.net/11245/1.238013.

[4] N. Costaras, in *A Changing Art Nineteenth-Century Painting Practice and Conservation* (Archetype Publications Ltd., London, 2017), pp. 14–22

[5] R. Frame, Materia: Journal of Technical Art History **2** (2022). https://issue-2.materiajournal.com/frame/.

[6] R. Marques, M. Sablier, J.J Boon, G. Rosé, L. Carlyle, I. Pombo Cardoso, and L. De Viguerie, Microchem. J. **181**, 107762 (2022). https://doi.org/https://doi.org/10.1016/j.microc.2022.107762.

[7] L. Carlyle, A Critical Analysis of Artists' Handbooks, Manuals and Treatises on Oil Painting Published in Britain Between 1800-1900: With Reference to Selected Eighteenth-Century Sources, University of London, 1991.

[8] L. Carlyle, The Conservator **17**, 56–60 (1993).

[9] M. Cotte, E. Checroun, J. Susini, and P. Walter. App. Phys. A: Materials Science and Processing **89** (4), 841–48 (2007). https://doi.org/10.1007/s00339-007-4213-4

[10] E. Joseph, C. Ricci, S. G. Kazarian, R. Mazzeo, S. Prati, and M. Ioele, Vib Spectrosc. **53** (2), 274–78 (2010). https://doi.org/10.1016/j.vibspec.2010.04.006

[11] S. Prati, E. Joseph, G. Sciutto, and R. Mazzeo, Acc. Chem. Res. **43** (6), 792–801 (2010). https://doi.org/10.1021/ar900274f

[12] E. Henderson, K. Helwig, S. Read, and S.M. Rosendahl, Heritage Science **7** (1), 1–15 (2019). https://doi.org/10.1186/s40494-019-0313-7.

[13] M. Noun, E. Van Elslande, D. Touboul, H. Glanville, S. Bucklow, Ph. Walter, and A. Brunelle, J. Mass Spectrom. **51** (12), 1196–1210 (2016) https://doi.org/https://doi.org/10.1002/jms.3885.

[14] C. Bouvier, S. Van Nuffel, P. Walter, A. Brunelle, J. Mass. Spectrom. **57**, 1: e4734 (2022) https://doi.org/https://doi.org/10.1002/jms.4734

[15] K. Keune, J.J. Boon, Anal. Chem. **76**, 1374−1385 (2004).

[16] V. Mazel, P. Richardin, D. Touboul, A. Brunelle, Ph. Walter, O. Laprévote, Anal. Chim. Acta **570** (1), 34-40 (2006)

[17] M. Cotte, T. Fabris, G. Agostini, D. Motta Meira, L. De Viguerie, V. A. Solé, Anal. Chem. **88**, 6154–6160 (2016)

[18] Q.P. Vanbellingen, N. Elie, M.J. Eller, S. Della-Negra, D. Touboul, and A. Brunelle, Rapid Commun. Mass Spectrom.: RCM **29** (13), 1187–95 (2015). https://doi.org/10.1002/rcm.7210

[19] C. Bouvier, H. Glanville, L. de Viguerie, C. Merucci, P. Walter, A. Brunelle, Anal Chem. **93** (10), 4463–71. (2021), https://doi.org/10.1021/acs.analchem.0c04471

[20] L. de Viguerie, P. A. Payard, E. Portero, Ph. Walter, and M. Cotte, Prog. Org. Coat. **93**, 46–60 (2016). https://doi.org/10.1016/j.porgcoat.2015.12.010

[21] J.D.J van den Berg, Analytical Chemical Studies on Traditional Linseed Oil Paints, University of Amsterdam, 2002.

[22] J. van der Weerd, A. Van Loon, and J. Boon, Stud. Conserv. **50**, 3–22 (2005). https://doi.org/10.2307/25487713

[23] M.R. Derrick, D. Stulik, and J.M. Landry, Infrared Spectroscopy in Conservation Science, Scientific Tools for Conservation (Los Angeles: The Getty Conservation Institute, 1999).

[24] E. Joseph, S. Prati, G. Sciutto, M. Ioele, P. Santopadre, and R. Mazzeo, Anal. Bioanal. Chem. **396** (2), 899–910 (2010). https://doi.org/10.1007/s00216-009-3269-8

[25] R. Marques, L. Carlyle, L. de Viguerie, I. Pombo Cardoso, and J.J. Boon in *Reflecting on Reconstructions, The Role of Sources and Performative Methods in Art Technological Studies. Proceedings of the Eighth Symposium of the ICOM-CC Working Group ATSR* (ICOM-CC, 2022), *pp.* 49–64.

[26] K. deGhetaldi, From egg to oil, the early development of oil painting during the Quatrocentto, University of Delaware, Department of Art Conservation, 2016

[27] K. Keune, E.S.B. Ferreira, and J.J. Boon. Triennial Meeting (14th), The Hague, 12-16 September 2005: Preprints, no. May 2014: 796–802 (2005). http://www.bcin.ca/Interface/openbcin.cgi?submit=submit&Chinkey=238594.

[28] E. Possenti, C. Colombo, M. Realini, C.L. Song, S.G. Kazarian, Anal. Bioanal. Chem. **413** (2), 455–67 (2021). https://doi.org/10.1007/s00216-020-03016-6

[29] V. Otero, D. Sanches, C. Montagner, M. Vilarigues, L. Carlyle, J. A. Lopes, and M. J. Melo, J. Raman Spectrosc. **45**, 11–12 (2014). https://doi.org/10.1002/jrs.4520

[30] L. Carlyle, The Artist's Assistant Oil Painting Instruction Manuals and Handbooks in Britain 1800-1900 With Reference to Selected Eighteenth-Century Sources (London: Archetype Publications Ltd, 2001).

[31] M.J. Plater, B. de Silva, T. Gelbrich, M.B. Hursthouse, C.L. Higgitt, D.R. Saunders, Polyhedron **22** (24), 3171–79 (2003). https://doi.org/10.1016/S0277-5387(03)00461-3

[32] J. Kirby, M. Spring, C. Higgitt, National Gallery Technical Bulletin **26**, 71–87 (2005). https://doi.org/10.1002/col.5080050319

[33] C. Bouvier, Étude du vieillissement de peintures anciennes par imagerie par spectrométrie de masse 3D, Sorbonne Université, 2022

[34] Y. Shimazu, Chemical and Optical Aspects of Appearance Changes in Oil Paintings from the 19th and Early 20th Century, University of Amsterdam, 2015.

[35] J. Boon, E.S.B. Ferreira, in *Reporting Highlights of the De Mayerne Programme* (The Hague, 2006), pp. 21–32.

[36] J.J. Boon, F.G. Hoogland, in *Issues in Contemporary Oil Paint* (Springer, Switzerland, 2014)